NUMERICAL DESIGN OF A BEAM-ENERGY-SPREAD MONITOR

Tsuyoshi SUWADA

KEK, High Energy Accelerator Research Organization
1-1 Oho, Tsukuba, Ibaraki, 305 Japan

Abstract

The KEKB injector linac is now being upgraded for the KEKB project. A beam-energy-spread monitor is under development in order to easily handle the beam orbits of primary high-current electron beams for producing a sufficient number of positrons. Paticularly, it is very useful to nondistructively control the energy spread at the entrance of the arc line in the linac. The author has proposed a multi-stripline-type energy-spread monitor in order to reinforce this purpose. This report describes the basic design of the monitor using a numerical analysis while taking account of the capacitive couplings between the beams and electrodes. The analysis result shows that the resolution($\Delta\sigma_E/E$) of the energy spread is expected to be 3×10^{-4} for the nominal operation conditions.

1. Introduction

The injector linac is required to stably accelerate primary high-current electron beams (6×10^{10}e/bunch) in order to produce a sufficient number of positrons for the KEKB rings[1]. The beam-position monitor is useful in order to easily handle the orbits of such high-current beams so as to suppress any beam breakup caused by large transverse wake fields. On the other hand, the beam-energy-spread monitor (BESM) is also important to suppress longitudinal wake fields and to stably transport the beams, especially at the arc line of the linac. In the linac design[2] for the KEKB, the new beam line is extended by about 225m in order to increase the beam energy by joining the old positron production line with an arc line. The primary high-current electron beams are accelerated to a beam energy of 1.5 GeV at the arc. The nominal value of the energy spread (σ_E/E) is designed to be 1.1% at the entrance of the arc. It is important to control this energy spread to be as small as possible in real-time operation, and to control the energy spread within a resolution on the order of 10^{-3} at least, for operators to easily handle the beam orbits.

2. Basic design and principle of the BESM

A multi-stripline-type BESM was proposed in order to easily monitor the energy spread at the arc and to realize a compact and simple monitor. The basic design of the monitor is shown in Fig.1. The monitor comprises a rectangular chamber with a horizontal length longer than the vertical one. Multiple electrodes are stretched on the inner surface of the chamber, where each electrode comprises a parallel stripline (50Ω) with the beam axis. The transverse sizes of the chamber have been decided to fully include transverse beam sizes. In the arc design, the chamber sizes are required to be 70$\times$30mm^2, taking into account beam sizes of 5σ, where the maximum sizes are

σ_x=7mm and σ_y=2mm on the nominal design[3]. The longitudinal length and width of the electrodes need to be decided from the viewpoint of the signal-to-noise ratio.

The principle of the monitor is simple. Let us assume two types of beams: one is a line beam and the other is a horizontally spread beam. If they pass through the chamber center, assuming that the total charge for each beam is the same, the electric potential on the central electrode induced by the line beam is larger than that induced by the spread beam, because the charge density of the line beam is larger than that of the beam spread around the central region. This means that if the width of the potential distribution induced on the multiple electrodes is measured at a bending section, the energy spread can be known because the horizontal beam width changes according to the horizontal dispersion.
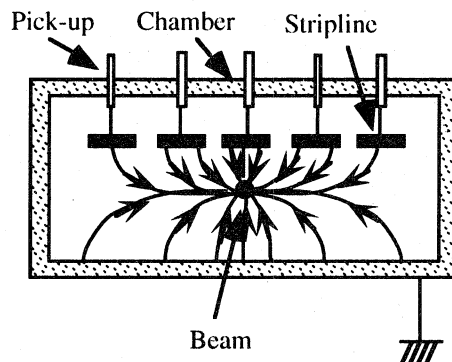

Fig. 1. Cross-sectional schematic view of the beam-energy-spread monitor. The beam-induced electric-field lines are also shown schematically.

3. Brief overview of the numerical method

A numerical analysis was carried out on the basis of a charge-simulation method[4,5]. Here, only a brief overview of this method is given in order to prepare for a discussion of the BESM analysis in the next section.

The electromagnetic fields generated by relativistic charged beams inside the vacuum chamber are almost boosted in the transverse direction to the beam axis due to Lorentz contraction. This phenomenon shows that the electromagnetic coupling of the electrodes to the beams can be well treated as a two-dimentional electrostatic potential problem. Thus, the BESM analysis is simply attributed to the electrostatic potential problem on the transverse plane. The charge-simulation method is based on the boundary element method for analyzing electrostatic potential problems. In this method, some boundary elements and imaginary charges are introduced in order to analyze an electrostatic-field system. All of the conductor surfaces in the system are divided into many domains, which are called "boundary elements"; imaginary charges are also arranged near to the boundary elements in a one-to-one manner. The

electrostatic potential of each conductor can be calculated so as to satisfy the boundary conditions of the system, that is, so as that the calculated equipotential surfaces correspond to the conductor surfaces by using the linear superposition of the electrostatic field contributed by all of the imaginary charges.

4. Application to the BESM

All of the surfaces of the chamber and electrodes are segmented as shown in Fig.2. The boundary elements on the chamber are arranged by using $n \times n$ elements with equal intervals in each vertical and horizontal direction, respectively. Each electrode surface is segmented by $m \times l$ elements (for the sake of simplicity, and the vertical element is fixed to be $l=2$). The segmentation numbers (n and m) are chosen based on the convergence of the electrostatic-field analysis. This method is guaranteed by the uniqueness of the solution on the electrostatic theorem.
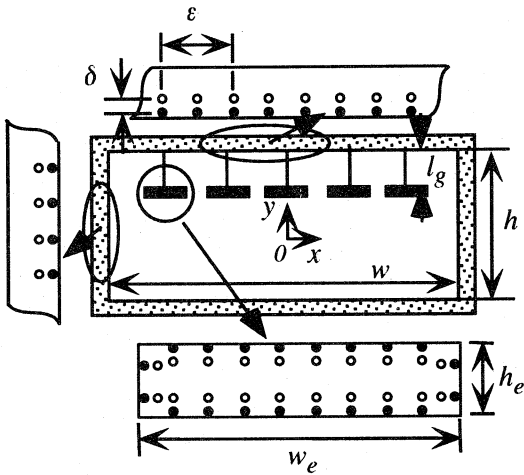

Fig. 2. Segmentation of the BESM chamber and electrodes. The black and open circles show the boundary elements and imaginary charges, respectively.

The rectangular coordinates (x_i, y_i) of the boundary elements on the chamber are given as:

$$x_i = w\left(\frac{1}{2} - \frac{1}{n}i\right), \qquad (4-1)$$

$$y_i = h\left(\frac{1}{2} - \frac{1}{n}i\right), \quad (1 \le i \le n). \qquad (4-2)$$

The coordinates (X_j, Y_j) of the imaginary charges are given as:

$$X_j = w\left(\frac{1}{2} - \frac{1}{n}j\right), \qquad (4-3)$$

$$Y_j = h\left(\frac{1}{2} \pm \frac{\delta}{h} - \frac{1}{n}j\right), \quad (1 \le j \le n). \qquad (4-4)$$

Here, w and h indicate the width and height for the inner surface of the chamber, respectively, and δ is the interval between the boundary element and the paired imaginary charge; the sign ($\pm$) is selected so that the imaginary charges are arranged inside the boundary elements(see

Fig.2). For the electrodes, the parameters $w_e(\leftarrow w)$, $h_e(\leftarrow h)$ and $m \times l(\leftarrow n \times n)$ are used. The parameter δ is given by

$$\delta = \varepsilon \times f, \qquad (4-5)$$

where ε is the interval between the adjoining boundary elements by a factor of 2 and f is a free parameter which must to be tuned (to be generally chosen within 0.2~1.5). The electrostatic potential (v_i^k) of the i-th boundary element in the k-th electrode ($k=0$ is assigned to the chamber) can be calculated by linearly superposing the potentials (v_{ij}) generated by all of the imaginary charges(q_j) and beam charge(q_{bj}), as follows:

$$v_i^k = \sum_j v_{ij}, \qquad (4-6)$$

$$= \sum_j P_{ij}q_j + \sum_j P_{ij}q_{bj}, \qquad (4-7)$$

$$P_{ij} = \frac{1}{2\pi\varepsilon_0}\ln\frac{1}{r_{ij}} + C, \qquad (4-8)$$

$$r_{ij} = \sqrt{(X_j - x_i)^2 + (Y_j - y_i)^2}, \qquad (4-9)$$

where P_{ij} and r_{ij} are the potential coefficient approximated for a line charge with infinite length, and the length between the i-th boundary element and the j-th imaginary (or beam) charge, respectively; ε_0 is the dielectric constant in the vacuum, and C the integration constant. The boundary conditions in this analysis are given as follows:
(a) The chamber potential (V_0) is equal to zero (ground potential),

$$V_0 = 0. \qquad (4-10)$$

(b) The charge summation on the k-th electrode is equal to zero,

$$\sum_i q_i^k = 0, \ (1 \le k). \qquad (4-11)$$

(c) The summation on the chamber charge (q_i^0) and the beam charge is conserved to be zero by the charge conservation,

$$\sum_i q_{bi} + \sum_j q_j^0 = 0. \qquad (4-12)$$

(d) The electrostatic potentials of the boundary elements in the same electrode are equal to the electrode potential (V_k),

$$V_k = v_i^k. \qquad (4-13)$$

Based on the above discussion, the electrode potentials are calculated by solving the above simultaneous linear equations (4.7) obeying boundary conditions ((4.10)~(4.13)).

5. Check of the numerical analysis

The goodness of the numerical analysis was investigated by analyzing the convergency of the

electrostatic potentials calculated for each electrode in various segmentation numbers (n and m), where a line charge with infinite length was assumed to be at the chamber center. The parameter f was tuned so as to produce good symmetrical and constant electrostatic potentials on the electrode surfaces. The segmentation numbers of $n=40$ and $m=5$ were obtained by a convergency calculation, the accuracy of which was deduced to be better than 1%. The parameters chosen based on the calculation are summarized in the following table.

Table 1. Several parameters used in the BESM analysis.

Chamber width w (mm)	70
Chamber height h (mm)	30
Chamber segmentation $n \times n$	40×40
Electrode width w_e (mm)	3
Electrode thickness h_e (mm)	1
Electrode segmentation $m \times l$	5×2
Number of electrodes	10
Gap length l_g (mm)	2
Chamber potential V_0 (Volt)	0
Beam charge (nC/mm)	1
Parameter f	0.6

6. Results of a numerical analysis

For the sake of simplicity, a numerical analysis was performed based on the variation in the width(1σ) of the horizontal spread charge at the chamber center. The spread charge was replaced by ten line charges arranged at regular intervals on the y-axis. The charge distribution was assumed to be a Gaussian function. It is useful to introduce the sensitivity (S) as follows:

$$S = \frac{\sigma_w}{(V_{peak}/\sum_i V_i)}, \qquad (6-14)$$

where σ_w is the width of the electrode potential distribution using the least-squared fitting of a Gaussian function, V_i and V_{peak} are the i-th electrode potential and the peak potential fitted.
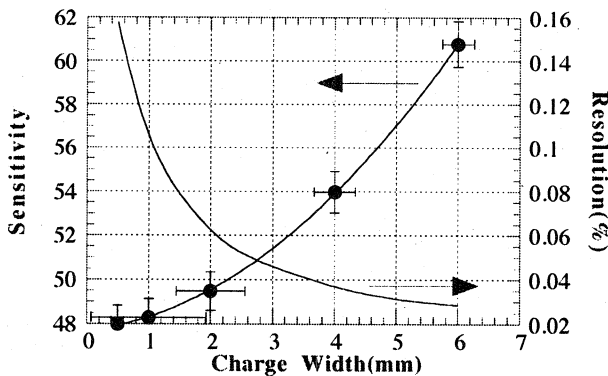

Fig. 3. Variations in the sensitivity and resolution of the energy spread depending upon the horizontal width of the charge.

Figure 3 shows the variation of the sensitivity and the resolution ($\Delta\sigma_E/E$) depending upon the charge width. The errors were derived by assuming errors of 1% in the electrode-potential measurement.

For example, an 8-bit digital oscilloscope is available to perform it. The resolution of the energy spread was derived from the horizontal dispersion of $\eta_x=9$mm/%. It is understood that the resolution strongly depends upon the horizontal beam size. Thus, the energy-spread measurement is advantageous at a large dispersion section. The horizontal beam size at a dispersion-maximum location around the center of the arc line is about $\sigma_x \sim 7$mm; for this beam size the resolution is expected to be 3×10^{-4}.

7. System design

A data-acquisition system (DAQ) is briefly described here. Figure 4 shows a schematic drawing of the DAQ system. The pick-up signal from each electrode is sent to a signal combiner after delaying a suitable time using cable-delay lines. Then, the combined signal is fed to a digital oscilloscope, which measures the peak voltage for the pulse-train signal.
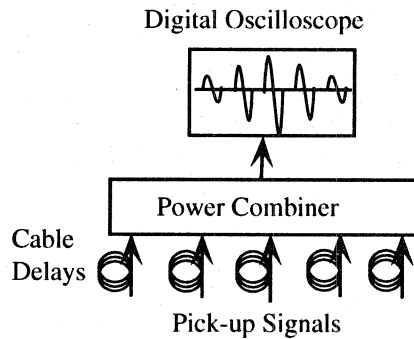

Fig. 4. Block diagram of the data-acqusition system of the BESM.

8. Conclusion

A new beam-energy-spread monitor was proposed by the author. The basic design of the monitor was formulated using numerical anaysis. The resolution of the energy-spread measurement is expected to be 3×10^{-4}. The resolution is sufficiently small to stably transport high-current beams and for operators to easily control them.

References

[1] S. Kurokawa, et al., KEK Report 90-24 (1991).
[2] I. Sato, et al., KEK Report 95-18 (1996).
[3] T. Kamitani, private communication.
[4] T. Kohno and T. Takuma, Numerical Calculation Method of Electric Field (CORONA, Tokyo, 1980).
[5] H. Singer, et al., IEEE Trans. Power Apparatus Syst. PAS-93, (1974) 1660.